Data-driven surrogates for predicting thermal performance and response functions of thermo-active piles

Javier Sánchez Fernández
Science and Solutions for a Changing Planet DTP, Imperial College London, London, UK, and Department of Civil and Environmental Engineering, Imperial College London, London, UK

Agustín Ruiz Lopez
Seequent, The Bentley Subsurface Company, Delft, Netherlands, and Department of Civil and Environmental Engineering, Imperial College London, London, UK, and

David Taborda
Department of Civil and Environmental Engineering, Imperial College London, London, UK

Abstract

Purpose – This paper develops fast, accurate data-driven surrogate models to predict the thermal performance and thermal response functions of single thermo-active piles. These replace computationally expensive finite element simulations and geometry-specific g-function calculations with generalisable machine-learning models suitable for preliminary design and performance assessment. This study aims to improve accessibility, reduce computational cost and support wider adoption of thermo-active piles within low-carbon and net-zero infrastructure strategies.

Design/methodology/approach – Two Artificial Neural Network surrogates were trained on databases generated from 3D transient finite element simulations of thermo-active piles. One surrogate predicts transient power output per unit length under a prescribed inlet fluid temperature, while the second predicts normalised pile wall and outlet thermal responses under constant heat flux. Input parameters were sampled using Latin Hypercube sampling. Model training used feature normalisation, cross-validation and regularisation, with performance evaluated using standard regression metrics and SHAP-based interpretability analysis.

Findings – Both surrogate models demonstrate excellent predictive accuracy and strong generalisation. The power output surrogate achieves R^2 values exceeding 0.99 with mean absolute errors typically below 2 W/m for most of the operational period. The thermal response surrogate reproduces pile wall and outlet g-functions over 10 years with global per-point R^2 values of 0.994–0.997 and per-timestep averages of 0.971 (wall) and 0.959 (outlet). Validation against a field thermal response test confirms reliable extrapolation beyond the trained diameter range. Computational time is reduced by several orders of magnitude compared with finite element analysis.

Originality/value – This study presents the first generalisable surrogate framework capable of predicting both power output per unit length and pile-specific g-functions for single thermo-active piles across a wide parameter space. By combining 3D numerical simulations with machine-learning surrogates and interpretability analysis, the work bridges the gap between physics-based modelling and practical engineering design. The approach provides a computationally efficient alternative to traditional thermo-active pile design methods.

Keywords Energy geotechnics, Thermo-active structures, Ground source energy, Thermal performance, Numerical analysis, Surrogate models, Artificial neural networks

Paper type Research paper

1. Introduction

Thermo-active structures are increasingly being adopted as part of the wider transition towards low-carbon and energy-efficient urban infrastructure. By integrating heat-exchange capabilities into existing foundation elements such as piles or diaphragm walls, renewable heating and cooling can be provided while eliminating the need for additional land use or

The current issue and full text archive of this journal is available on Emerald Insight at: **https://www.emerald.com/insight/3029-0414.htm**

Machine Learning and Data Science in Geotechnics
2/1 (2026) 173–185
Emerald Publishing Limited [ISSN 3029-0414]
[DOI 10.1108/MLAG-01-2026-0002]

Funding: This research is part of the SaFEGround (Sustainable, Flexible and Efficient Ground-source heating and cooling systems) project, which is funded by the Engineering and Physical Sciences Research Council (EPSRC) (grant number: EP/V042149/1), and part of the SIDeTools (Sustainable Infrastructure Design Tools) project, funded by the Engineering and Physical Sciences Research Council (EPSRC) (grant number: EP/X52556X/1). This work was also supported by the Natural Environment Research Council [NE/S007415/1].

Received 27 January 2026
Revised 14 May 2026
Accepted 22 June 2026

construction demands. As cities and countries move towards net-zero carbon targets, ground source heat pump systems implemented through thermo-active foundations offer an attractive alternative to supply total or partial heating and cooling demand of buildings (Laloui *et al.*, 2006; D'Agostino *et al.*, 2020).

Despite their advantages, the design of thermo-active piles remains technically demanding. Current methodologies typically rely on detailed numerical modelling or on semi-analytical approaches that require expert judgement and significant computational effort. These methods must account for the interaction between the pile, the working fluid and the surrounding soil, as well as the transient nature of heat transfer. While such approaches are well established and reliable, they are time-consuming to apply, difficult to generalise and often impractical during the early design stages where rapid decision-making is required (Bourne-Webb *et al.*, 2016).

To address these challenges, considerable research has focused on simplifying the representation of pile heat exchangers. A major development in this regard is the adoption of g-functions, previously used for the design of borehole heat exchangers. These are normalised thermal response functions that relate temperature change to time through a non-dimensional Fourier number (Eskilson, 1987; Loveridge and Powrie, 2014). G-functions provide an efficient means of capturing the thermal behaviour of borehole and pile heat exchangers, with a significantly reduced computational cost compared with full finite element (FE) analysis. Their use has also been adapted for the design of pile groups (Liu and Taborda, 2024b). However, as g-functions remain strongly dependent on geometry, material parameters and flow conditions, generating new sets typically requires high-fidelity numerical simulations. This limits their generality and restricts their integration into optimisation workflows or early-stage design studies.

In parallel, recent advances in machine learning are transforming how complex physical systems can be simulated and approximated, with successful applications across a range of civil engineering problems including structural dynamics, soil-structure interaction and geotechnical design optimisation. Within the specific context of energy piles, existing data-driven approaches have targeted either steady-state thermal resistance (Imtiyaz *et al.*, 2023), short-duration outlet temperatures for narrowly parametrised or fixed installations (Zhang *et al.*, 2023; Wang *et al.*, 2025), or geometry-specific surrogates that require a new simulation each time pile geometry or material properties change (Makasis *et al.*, 2018). None of these studies span the full design parameter space, including pile geometry, soil and concrete thermal conductivity, pipe configuration and fluid velocity, nor produces the normalised thermal response functions required for integration into superposition-based design workflows.

To date, therefore, no generalisable surrogate framework has been developed to predict the full transient thermal performance of a single thermo-active pile across a wide range of geometrical, material and hydraulic parameters. The present work addresses this gap by introducing two complementary surrogate models trained on data from high-fidelity FE thermal simulations. The first surrogate predicts the evolution of power output per unit length of a thermo-active pile during one year of operation. The second surrogate provides the normalised thermal response functions based on the average pile wall (Φ_{wall}) and outlet fluid (Φ_{outlet}) temperatures over 10 years, enabling direct computation of g-functions for a wide range of geometries and material properties. These surrogates offer a generalisable, computationally efficient framework for the rapid assessment and preliminary design of thermo-active piles, removing the need for repeated FE simulations and enabling systematic exploration of the design space across a wide range of geometrical, material and hydraulic configurations.

2. Methodology

2.1 Finite element models

To generate the numerical database for surrogate model training, a parametrised 3D FE thermal model was developed in COMSOL Multiphysics combining transient heat transfer in solids and pipes. The parametric models share a common geometry, with a single pile with varying radius and length, embedded on a cubic soil domain with dimensions $80 \times 80 \times (L_{pile} + 20)$ m. The initial condition is a uniform ground temperature across all domains (Loveridge and Powrie, 2013; Makasis *et al.*, 2020). Outer soil boundary conditions are assigned a Dirichlet boundary condition, where $T = T_{initial}$.

A layered stratigraphy with three soil types of randomised thickness and thermal conductivities is adopted. All soils have an assumed density ρ_{soil} of 2650 kg m^{-3} and volumetric heat capacity of 1800 kJ m^{-3} K^{-1}. According to Zhang *et al.* (2025), based on the conclusions of a computational study, the thermal resistance of the pile-soil interface may have a measurable impact on its thermal performance. However, given the difficulty associated with the quantification of this parameter, particularly at the design stage, perfect pile-soil contact was assumed. This approach is in line with previous studies reproducing field measurements of temperature fields around ground heat exchangers [see e.g. Gawecka *et al.* (2017) and Gawecka *et al.* (2020)].

The absorber pipes are arranged in either one, two, three or four loops and they are connected in a chain, such that a single global inlet and global outlet exist (see Figure 1). These are modelled with linear elements with incorporated advection and conduction in the FE formulation. The pipes are placed equally around the pile radius, maintaining an equal distance among the pipes and allowing for 70 mm cover, as shown in Figure 1. The heat exchanger fluid is assumed to be water, with its respective values of specific heat capacity $C_{p,w}$ of 4.18 kJ kg^{-1} K^{-1}, a density ρ_w of 1000 kg m^{-3}. The fluid flow inside the pipe with an area A_{pipe} corresponding to a diameter of 26.2 mm was assumed frictionless and simulated with a fluid velocity, v_{fluid}, varied parametrically. This assumption is justified, as frictional heating in smooth plastic pipes is negligible relative to the prescribed heat exchange rates at the fluid velocities considered, even under turbulent flow conditions (Cecinato and Loveridge, 2015). Furthermore, as fluid velocity is prescribed directly as a model input, head losses are not considered in the performed analysis.

To generate the two types of surrogate models, two distinct modelling approaches were followed, as illustrated in Figure 2. To determine the power output per unit length, a constant temperature, T_{inlet}, was prescribed at the global inlet of the pile. Global outlet temperatures were recorded from initial

Figure 1 Pipe arrangement for different U-loops in a pile cross section

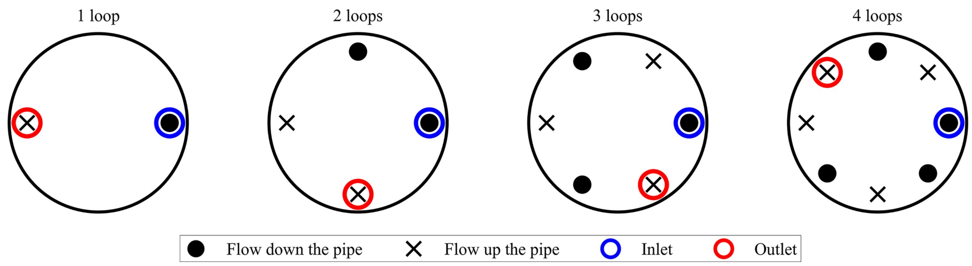

Figure 2 Schematic of (a) soil deposit and pile geometry, (b) power output pile and (c) thermal response pile

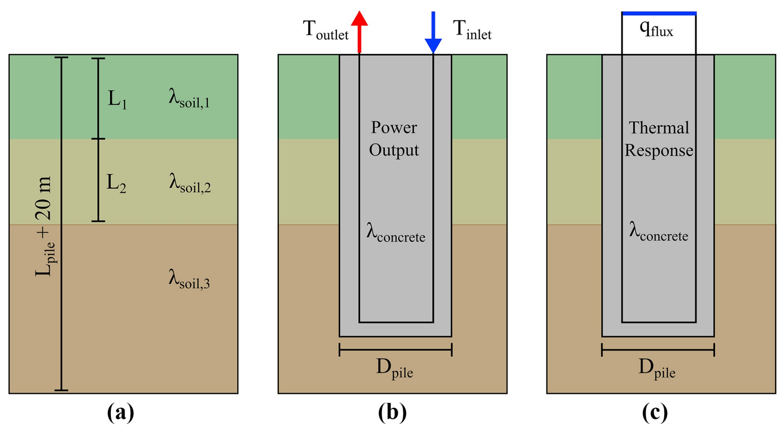

conditions up to 360 days, plus an additional steady-state temperature value to establish the long-term performance of the pile, obtained from a separate steady-state analysis. The power output [W] can be determined, as shown in Liu and Taborda (2023), using:

$$P = \rho_w C_{p,w} \cdot v_{fluid} \cdot A_{pipe} \cdot (T_{inlet} - T_{outlet}) \tag{1}$$

In the second type of surrogate model, which assesses the thermal response of the pile, a constant rate of heat extraction q_{flux} $[W]$ was applied to the pipe connecting the global outlet and inlet of the piles. The average temperature of the pile, calculated at each time instant by integrating the temperature field over the pile surface, and the temperature at the global outlet of the pile were recorded for the first 10 years of operation at time instants that are equally spaced in a logarithmic scale.

The numerical models combine two different transient physics: heat transfer in the solid domain (soil and pile) and heat transfer in pipes, following the formulation in COMSOL Multiphysics (2021). Equation (2) describes the former, assuming a conduction-only heat transfer, in line with the approach taken for thermo-active piles installed in low-permeability materials or deposits characterised by relatively low groundwater seepage velocities (Bourne-Webb *et al.*, 2013; Bourne-Webb *et al.*, 2016):

$$\rho C_p \frac{\partial T}{\partial t} = \lambda \cdot \nabla^2 T + Q \tag{2}$$

where ρ is the material density, C_p is the specific heat capacity and Q (W·m^{-3}) is a sink/source term. Equation (3) describes heat transfer in pipes, including both conduction and advection, following the assumption of negligible frictional heating (COMSOL Multiphysics, 2021):

$$\rho_w \cdot A_{pipe} \cdot C_{p,w} \cdot \frac{\partial T}{\partial t} = A_{pipe} \cdot \lambda_w \cdot \nabla^2 T - \rho_w \cdot A_{pipe} \cdot C_{p,w} \cdot v_{fluid} \cdot \nabla T + Q_{wall} \tag{3}$$

where ρ_w, $C_{p,w}$ and λ_w are the water density, specific heat capacity and thermal conductivity, v_{fluid} is the fluid velocity and Q_{wall} (W·m^{-1}) is a term representing heat transfer through the wall. Given the narrow temperature range, all material properties can be assumed to be temperature independent (Gawecka *et al.*, 2020).

The computational domain was discretised in COMSOL using quadratic tetrahedral elements for all 3D domains, with the pipe network represented by 1D elements. To resolve accurately the steep thermal gradients, the mesh was refined near the pipe heat exchanger and the immediate vicinity of the pile wall. Due to variations in pile geometry, the number of elements in the finite element meshes varied between 100,000 and 500,000.

2.2 Numerical data

Eight hundred numerical analyses were computed for each of the two databases – power output and thermal response –, with 200 analyses assigned to each of the four pipe loop configurations ($n_{loops} = 1,2,3,4$). The inputs of these analyses were sampled using Latin Hypercube sampling (McKay *et al.*, 1979) to ensure consistent and uniform coverage of the input space compared to random sampling techniques. All sample combinations, defined in Table 1 in terms of the range of parameters sampled for each of the numerical models, were computed successfully. The selected parameter ranges accommodate diverse pile configurations, ensuring the applicability and generalisability of the two surrogate models. Figure 3 illustrates, for all samples in the two data sets, the calculated distributions of inlet-outlet temperature [power output surrogate, Figure 3(a)], and pile wall and outlet temperatures [thermal response surrogate, Figures 3(b) and (c), respectively]. In Figure 3(a), where a constant inlet temperature is applied, most series of ΔT converge toward an asymptotic value between 2 °C and 5 °C, reflecting the reduction in thermal gradients within the system as it approaches steady-state conditions. The temperature range is wider for the constant applied heat flux database, with the majority of wall [Figure 3(b)] and outlet [Figure 3(c)] temperature differences varying between 5 °C and 20 °C.

3. Surrogate model

3.1 Data preprocessing

The obtained data from the FE models was postprocessed and prepared for use as database for creating the regression surrogates. The three thermal conductivities for the layered soil were combined into a single weighted average value, $\lambda_{soil,avg}$, for each of the samples, as shown in equation (4). This simplification is motivated by the predominantly radial nature of heat transfer from a vertical pile in horizontally stratified soil, where each layer contributes independently and proportionally to its thickness along the pile length, resulting in a reduction in input dimensionality from five parameters describing the layered system to a single scalar. It should be noted that this averaging is applied only as a pre-processing step during surrogate input construction; the FE simulations fully resolve the three-layer stratigraphy, and the surrogate is therefore trained on outputs that inherently reflect the full layered soil behaviour. Therefore, the surrogate models have the pile length and diameter, concrete and average soil thermal conductivities, initial temperature, fluid velocity and number of pipe loops as common inputs. These are in addition to the constant inlet temperature, T_{inlet}, for the model calculating the power output per unit length of pile, or the normalised heat flux extracted by the heat pump, $\overline{q_{flux}}$ [W·m^{-1}], in the case of the thermal response surrogate:

$$\lambda_{soil,avg} = \lambda_{soil,1} \cdot \frac{L_1}{L_{pile}} + \lambda_{soil,2} \cdot \frac{L_2}{L_{pile}} + \lambda_{soil,3} \cdot \left(1 - \frac{L_1 + L_2}{L_{pile}}\right) \tag{4}$$

For piles subjected to a constant inlet temperature, the outlet temperature is computed for 16 time instants approximately logarithmically spaced within the first 360 days of operation, plus the additional steady state temperature, representing the long-term thermal performance of the pile (total of 17 outputs). The resulting power output per unit length, P [W·m^{-1}], which is the desired prediction of the power output surrogate, can be calculated as:

$$P(t) = \frac{\rho_w C_{p,w} v_{fluid} A_{pipe} (T_{outlet}(t) - T_{inlet})}{L_{pile}} \tag{5}$$

Conversely, the second surrogate predicts the normalised thermal response (Φ) for the average pile wall temperature (Φ_{pile}) and the outlet temperature (Φ_{outlet}) at 120 time instants logarithmically spaced within the first 10 years of operation (total of 240 outputs). These are calculated from the temperature values $T_{pile,avg}$ and T_{outlet}, respectively, as shown in equations (6) and (7). When the normalised thermal response is shown in conjunction with the Fourier number [equation (8)], or dimensionless time, it is formally referred to as the g-function (Loveridge and Powrie, 2013):

$$\Phi_{pile}(t) = 2\pi \cdot \frac{\lambda_{soil,avg}}{\overline{q_{flux}}} \cdot \left(T_{initial} - T_{pile,avg}(t)\right) \tag{6}$$

$$\Phi_{outlet}(t) = 2\pi \cdot \frac{\lambda_{soil,avg}}{\overline{q_{flux}}} \cdot \left(T_{initial} - T_{outlet}(t)\right) \tag{7}$$

$$Fo = \frac{\lambda_{soil,avg} \cdot t}{\rho_{soil} C_{p,soil} \cdot r_{pile}} \tag{8}$$

3.2 Model architecture

The surrogate models were developed using feedforward artificial neural networks (ANNs) implemented with the Keras API within the TensorFlow framework (Chollet, 2021). These

Table 1 Finite element model parameters

Parameter	Lower bound	Upper bound	Unit	Description
L_{pile}	15	45	[m]	Pile length
D_{pile}	0.5	2	[m]	Pile diameter
$\lambda_{soil\ 1,2,3}$	0.5	5.0	[W m^{-1} K^{-1}]	Thermal conductivity of soil layer 1, 2 and 3
$\lambda_{concrete}$	0.5	5.0	[W m^{-1} K^{-1}]	Thermal conductivity of concrete
L_1/L_{pile}	0.15	0.45	[-]	Ratio of soil layer 1 thickness to pile length
L_2/L_{pile}	0.15	0.45	[-]	Ratio of soil layer 2 thickness to pile length
$T_{initial}$	10	20	[°C]	Initial temperature
n_{loops}	1	4	[-]	Number of loops
v_{fluid}	0.1	1.0	[m s^{-1}]	Pipe fluid velocity
T_{inlet}	0	8	[°C]	Inlet temperature (Surrogate 1)
$\overline{q_{flux}}$	−10	−80	[W m^{-1}]	Normalised heat flux (Surrogate 2)

Figure 3 Evolution of (a) the difference between outlet and inlet (constant) temperatures, (b) the wall-averaged temperature, and (c) the outlet temperature, over time for all samples in the database

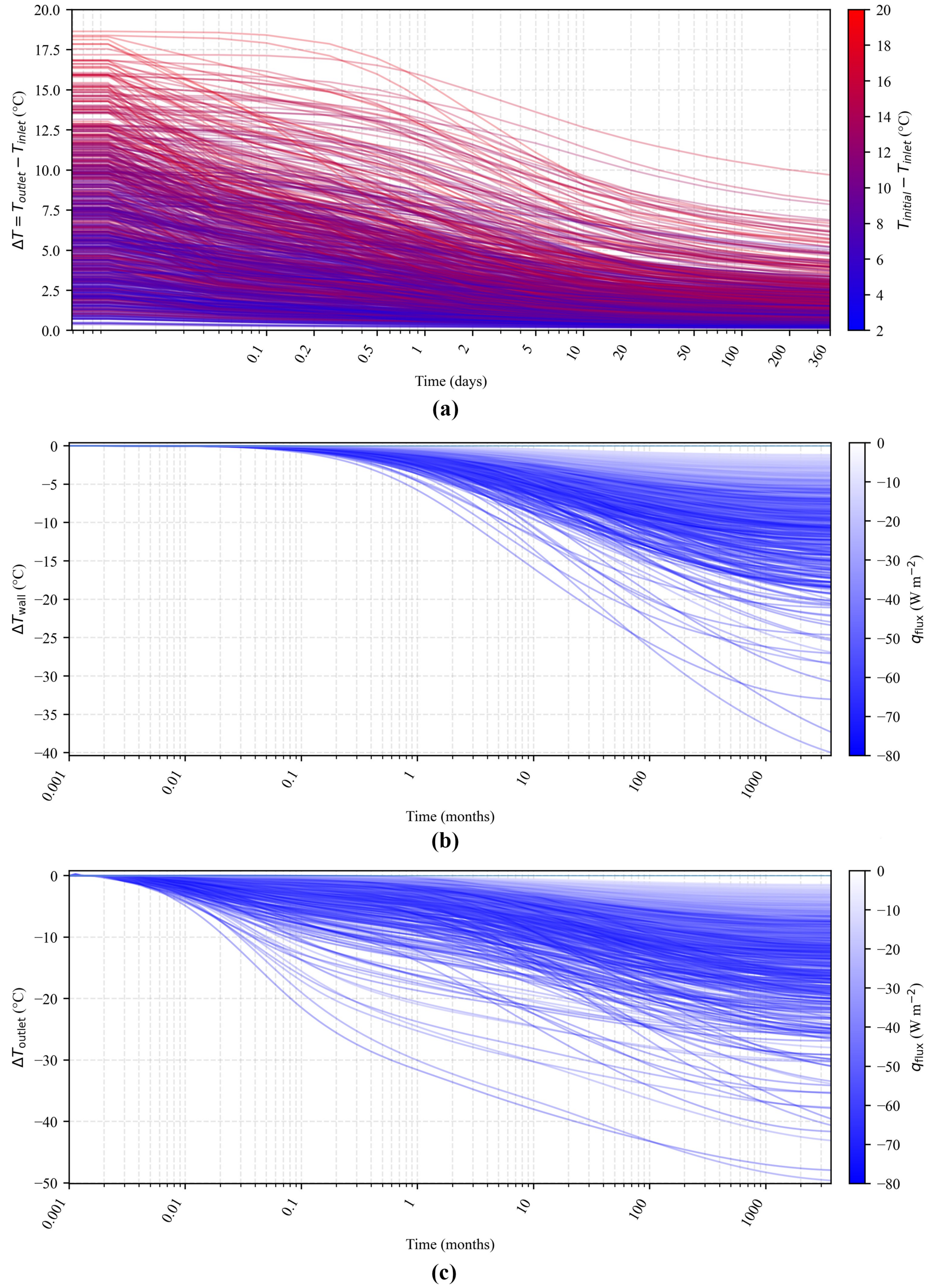

were selected as a practical compromise between predictive accuracy, computational efficiency and flexibility. Their ability to handle high-dimensional inputs, multiple simultaneous outputs and non-linear relationships across a wide parameter space makes them well suited to the regression problems considered in this study. The architecture consists of three hidden dense layers with ReLU (Rectified Linear Unit) activation functions, followed by dropout layers and a linear activation function for the output regression layer. To improve training stability, each hidden layer is followed by a Batch Normalisation layer. The input data set was partitioned into training (80%), validation (10%) and testing (10%) sets, with both input features and output labels being normalised using *StandardScaler* (Geron, 2019). A 10-fold cross-validation scheme was implemented to systematically tune key hyperparameters, including the number of neurons in each hidden layer, the dropout rate and the batch size. The full list of hyperparameter values considered and the best combination for each surrogate is provided in Table 2. The two models were trained using the Adam optimiser to minimise the mean

Table 2 Hyperparameter grid used for model training

Hyperparameter	Values studied	Surrogate 1	Surrogate 2
Dropout rate	0.1, 0.2, 0.3, 0.4	0.2	0.3
Batch size	10, 20, 30, 40, 80	40	30
Layer 1 Neurons	2048, 1024, 512	1024	512
Layer 2 Neurons	512, 256, 128	256	512
Layer 3 Neurons	256, 128, 64	128	256

squared error loss function for a maximum of 500 epochs. To ensure robust convergence and prevent overfitting, two Keras callbacks were used: the learning rate was progressively reduced by a factor of 0.8 for every 8 epochs without improvement in the validation loss, while an *EarlyStopping* callback terminated training if the validation loss failed to improve for 20 consecutive epochs, restoring the model weights to those from the best-performing epoch. Figure 4 shows both model's architecture and final parameters used during the training process.

4. Surrogate model results

The trained surrogate models are shown to accurately predict the thermal behaviour of a single thermo-active pile, while reducing the computational time by several orders of magnitude. The FE database, comprising 800 different samples for each model, required approximately two weeks to generate, with an average solution time of 25 min per sample. In contrast, a trained surrogate provides a prediction in a fraction of a second, achieving a computational speed-up of over five orders of magnitude.

This section presents a detailed performance analysis of the two models developed: the power output surrogate, which predicts the transient heat exchange rate given a fixed inlet temperature, and the thermal response surrogate, which predicts the pile wall and outlet temperature evolution under a constant heat flux boundary condition.

Figure 4 ANN surrogate models architecture

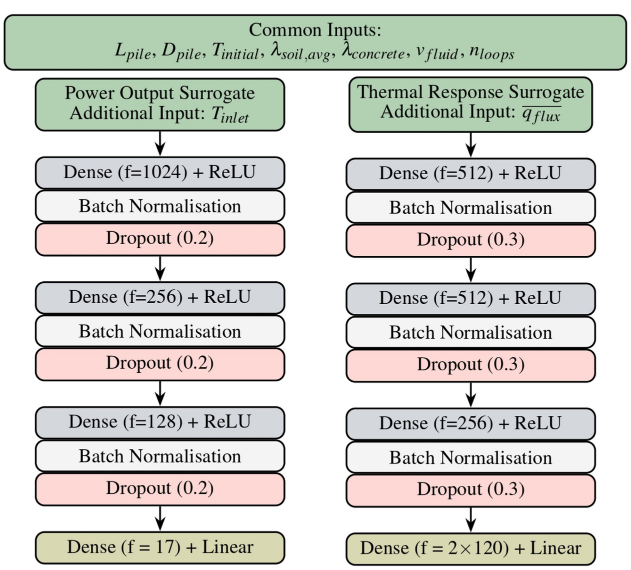

4.1 Power output surrogate predictions

The overall results for the training, validation and test data sets, shown in Figure 5, demonstrate the capabilities of the surrogate model at determining the power output with minimal overfitting. The model achieves a coefficient of determination (R^2) of 0.997 on the training set and demonstrates excellent generalisation with R^2 values of 0.992 and 0.993 on the validation and test sets, respectively. The mean absolute error (MAE) on the unseen test data is 4.37 W/m, with significantly lower values for larger time instants, as shown later. The corresponding mean relative error (MRE) is 4.4%, indicating high predictive fidelity across the entire range of output values. The close agreement between the performance on the training and test sets confirms that the model is robust and has learned the underlying relationships rather than memorising the training data.

To examine the model's performance, Figure 6 illustrates the surrogate's ability to replicate the full transient power output curve for specific test cases. The samples shown were selected to be representative of the 25th (low error), 50th (median error) and 75th (high error) percentiles of the MAE across the test set. In all three cases, there is good agreement between the real and predicted values across all time instants. The largest errors tend to occur at the start of the simulation ($t < 1$ *day*), where the thermal response is most transient, although this is of limited consequence for practical design use, as performance assessments and seasonal load estimations are governed by medium to long-term behaviour. The model successfully captures the steep decline in power output at early times, followed by a gradual stabilisation. This confirms that the surrogate is not just accurate on average, but can also predict reliably the operational profile for any specific pile configurations.

The model's accuracy is further evaluated at discrete time instances on the test set, to assess its ability to capture the thermal response over time, as shown in Figure 7. The surrogate maintains high accuracy throughout the simulation period. For the short-term prediction at Day 1, characterised by steep thermal gradients, the model achieves an R^2 of 0.989. The performance is similarly high for medium- and long-term predictions, with R^2 scores of 0.994 and 0.990 for Day 30 and Day 360, respectively.

4.2 Thermal response g-functions surrogate predictions

The second surrogate was trained to predict the transient wall and outlet normalised responses. As shown in Figure 8, both outputs of this surrogate demonstrate excellent agreement with the reference FE results, with predictions tightly clustered around the 1:1 line. When considering the global, per-point accuracy, coefficients of determination R^2 of 0.994–0.997 are achieved. For the average per-timestep accuracy, R^2 values of 0.971 for the wall thermal response and 0.959 for the outlet thermal response are obtained.

Figure 9 shows the evolution of the MAE and root mean squared error (RMSE) for both wall and outlet thermal responses. The errors remain consistently low during the early transient phase, when steep temperature gradients dominate the system behaviour. The MAE stays below 0.05 and 0.1 for the wall and outlet respectively up to approximately

Machine Learning and Data Science in Geotechnics
Volume 2 · Number 1 · 2026 · 173–185

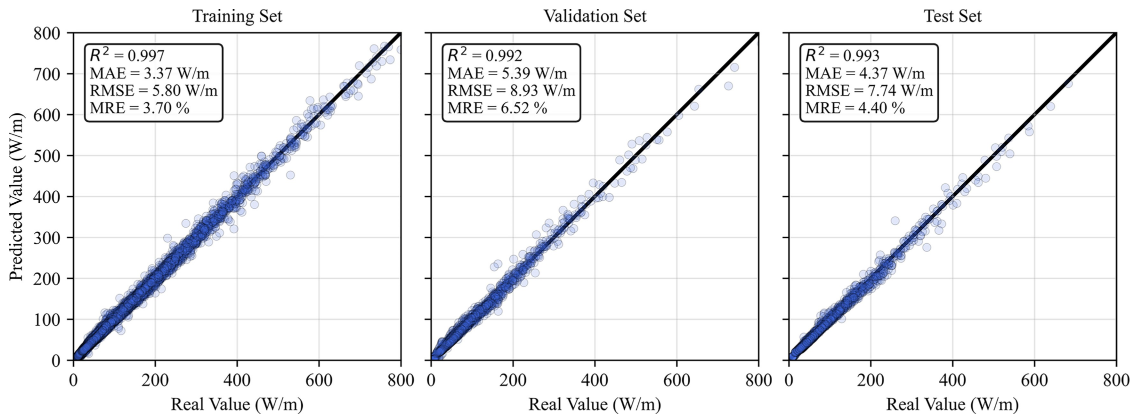

Figure 5 Surrogate predictions against real power outputs for the training, validation and test sets

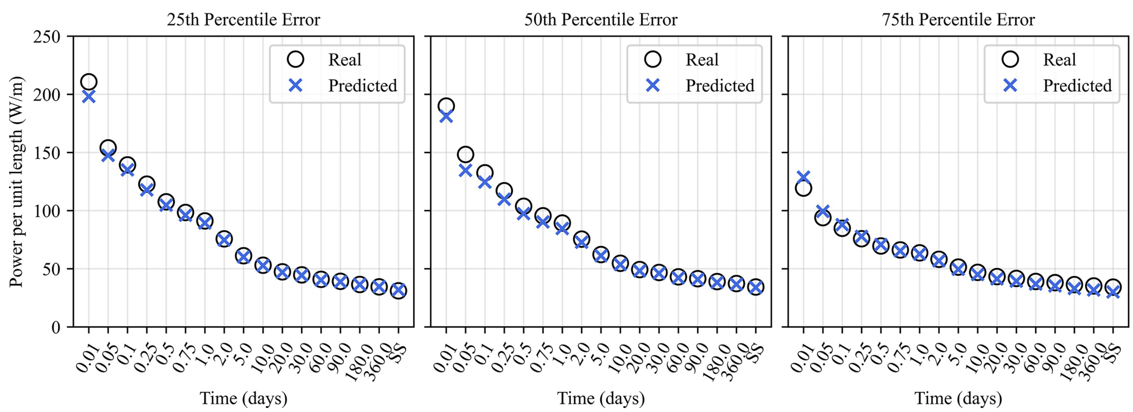

Figure 6 Real vs predicted power output for samples at the 25th, 50th and 75th percentiles of the mean absolute error (MAE)

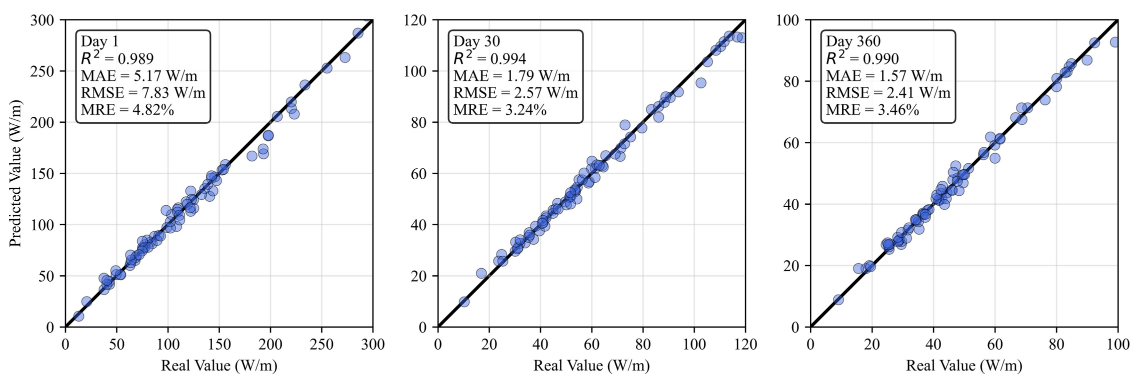

Figure 7 Surrogate test set predictions after 1, 30 and 360 days of continuous operation

10^{-1} months (≈ 3 *days*), indicating excellent short-term fidelity. The close agreement between the MAE and RMSE curves throughout the entire time domain suggests a minimal presence of outliers. As time progresses, both metrics exhibit a gradual absolute increase as the predicted values of Φ_{wall} and Φ_{outlet} also increase. In terms of relative error, values of the MRE remain very low – generally between 3% and 5% – for both surrogates throughout the entire analysis, including steady state.

A more detailed assessment of the surrogate's performance for individual samples is presented in Figure 10, for cases corresponding to the 25th, 50th and 75th percentiles of the RMSE (used to evaluate the loss function). Across the three selected examples, the predicted curves follow the real g-function values closely, reproducing both the initial steep rise and the subsequent asymptotic trend. The differences that emerge towards the end of the simulation are small and remain consistent across the three analyses. This behaviour

Figure 8 Overall predicted against real values for all test datapoints for (a) wall and (b) outlet temperatures

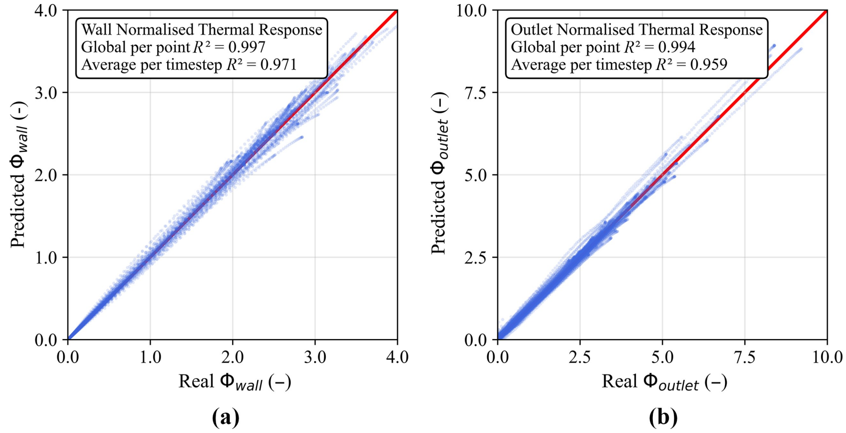

Figure 9 Variation of MAE and RMSE with time for (a) wall and (b) outlet temperatures

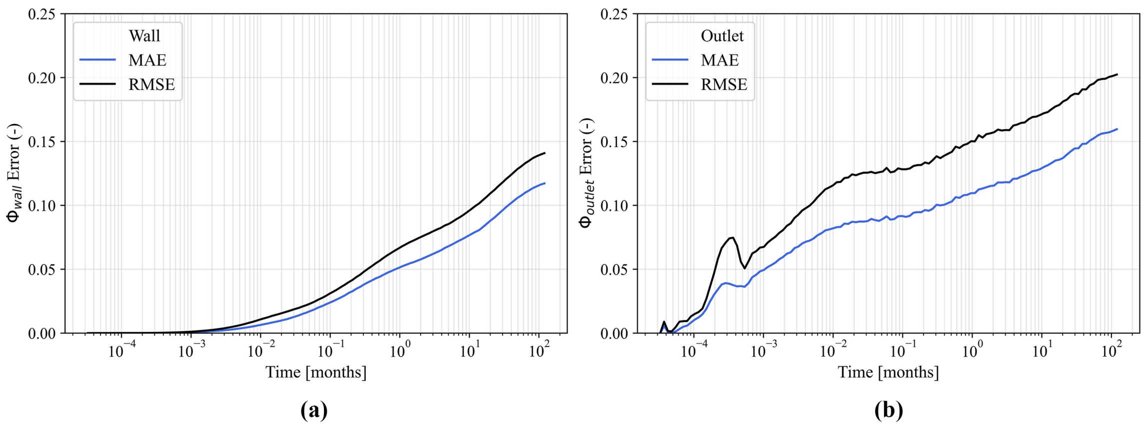

Figure 10 Real vs predicted g-function for samples at the 25th, 50th and 75th percentile of the RMSE

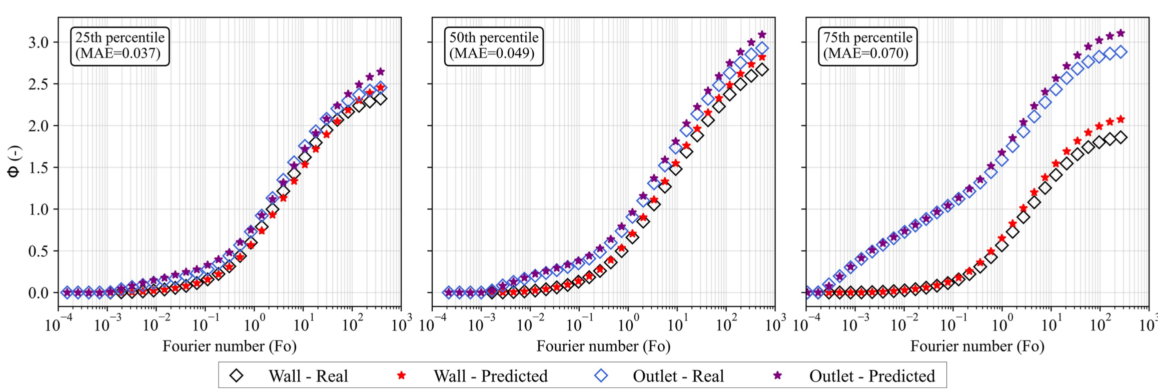

is attributed to the gradual transition of the physical problem from a predominantly 2D regime, governed by radial heat diffusion around the pile, to a 3D regime at later times for which vertical heat flux becomes more significant. While the numerical FE model fully captures this transition, the surrogate has a limited ability to infer these subtle multi-dimensional effects and can only approximate it based on the available training data. Nevertheless, the predictive errors remain small and well within acceptable engineering bounds.

5. Feature importance analysis

While ANNs are powerful tools for creating accurate surrogate models, their complex, non-linear structure often results in a "black box" nature. Unlike analytical models, ANNs lack a direct, standard method for quantifying the importance of individual input features. Furthermore, high R^2 values for the testing data set such as those reported above are consistent both with a surrogate that reflects the underlying physical mechanisms and with one that has exploited strong input-output correlations without having learned physically meaningful relationships. Indeed, given the strong physical constraints inherent to conductive heat transfer in thermo-active piles, high predictive accuracy is arguably an expected minimum rather than a distinguishing achievement. Consequently, R^2 alone provides limited basis for confidence in the surrogate's physical fidelity, and post hoc model interpretation is necessary to assess whether the learned input–output relationships are physically meaningful. For this study, we use SHAP (Shapley Additive Explanations), a game theory-based approach that explains the output of any machine learning model by assigning each feature an importance value for a particular prediction (Lundberg and Lee, 2017). The SHAP explanation for a single prediction is expressed as a linear model of feature contributions:

$$f(\mathbf{x}_k) = \phi_{k,0} + \sum_{i=1}^{N} \phi_{k,i} \tag{9}$$

where $f(\mathbf{x}_k)$ is the model's prediction for the k-th feature vector $\mathbf{x}_k$, $\phi_{k,0}$ is the corresponding baseline prediction (the mean model prediction for the k-th feature over the entire data set), N is the number of features and $\phi_{k,i}$ is the SHAP value of feature i for the k-th sample, representing its contribution to the final prediction. The mean absolute SHAP values for each feature i, across all samples K in the test set, can be obtained as:

$$I_i = \frac{1}{K} \sum_{k=1}^{K} |\phi_{k,i}| \tag{10}$$

and provide a robust measure of global feature importance, allowing the ranking of input parameters by overall impact on the predicted response.

Figure 11 shows the mean absolute SHAP values for the power output surrogate model. To highlight the differences in feature importance between short- and long-term conditions, this is evaluated at two phases: the transient phase at Day 1 and the steady state. The results have been ranked by the relative importance of the steady-state SHAP values. As expected, the temperature difference $T_{inlet} - T_{initial}$ is the most influential feature for driving the model prediction under both conditions, as it determines directly the rate of heat exchange between the heat carrier fluid and the pile-soil system throughout all stages of operation.

The number of loops (n_{loops}) consistently exhibits a strong influence in both the transient and steady-state conditions, as it directly affects the effective heat transfer area and the total flow path available for energy exchange. The pile length L_{pile}, on the other hand, plays a relatively minor role since the surrogate predicts power output normalised per unit length; its contribution would be more substantial if total power output were considered. Finally, the fluid velocity (v_{fluid}) shows greater relevance during the transient phase, when large thermal gradients enable higher flow rates to enhance energy extraction. At steady state, once temperature differences stabilise, variations in flow velocity have a smaller effect on the overall power output.

In the early transient regime, the system response is dominated by heat conduction within the pile itself, leading to $\lambda_{\mathrm{concrete}}$ having significant influence on the power output prediction. This behaviour is consistent with the thermal diffusion length scale $\delta(\mathrm{t}) = \sqrt{\alpha \cdot \mathrm{t}} = \sqrt{\frac{\lambda}{\rho \mathrm{c_p}}\mathrm{t}}$, defined as the characteristic distance over which a thermal disturbance propagates through a medium of diffusivity α in time t. In an idealised system where the heat source coincides with the axis of the thermos-active pile, δ remains small relative to the pile radius at early times, indicating that the thermal front is largely confined within the pile and that the internal concrete resistance governs the instantaneous power output. As δ extends beyond the pile boundary, $\lambda_{\mathrm{soil,avg}}$ begins to gain importance as a resistance to heat dissipation, ranking second in importance under steady-state conditions. This transition corresponds physically to the Fourier number $\mathrm{Fo} = \alpha \mathrm{t}/\mathrm{r}_{\mathrm{pile}}^2$, increasing to values greater than one. To illustrate this process for the analysed problem, the characteristic time $\mathrm{t}^* = \mathrm{r}_{\mathrm{pile}}^2/\alpha_{\mathrm{concrete}}$, which corresponds to $\delta = \mathrm{r}_{\mathrm{pile}}$, was computed for each test sample, yielding a mean of $\mathrm{t}^* = 6.4$ days. Figure 12 shows, as continuous functions of time, the mean absolute SHAP importance of $\lambda_{\mathrm{concrete}}$ and $\lambda_{\mathrm{soil,avg}}$ normalised by their respective maximum values to enable a direct comparison, together with the mean t^* and the boundaries $\delta = \mathrm{r}_{\mathrm{pile}}/2 \Rightarrow \mathrm{t} = \mathrm{t}^*/4$ and $\delta = 3\mathrm{r}_{\mathrm{pile}}/2 \Rightarrow \mathrm{t} = 9\mathrm{t}^*/4$. Clearly, the importance of $\lambda_{\mathrm{concrete}}$ decreases as t^* increases, consistent with the thermal front progressively

Figure 11 Mean absolute SHAP contribution for the input features for the Day 1 output (left) and steady-state (right)

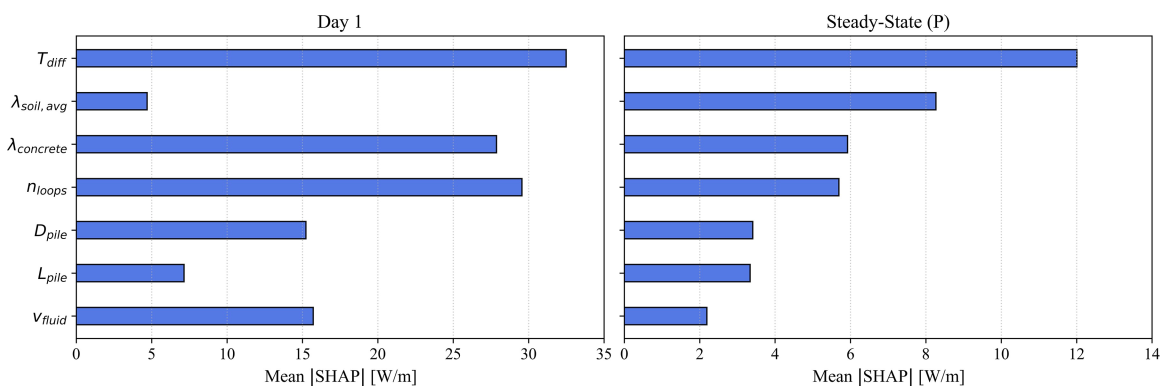

Figure 12 Normalised mean absolute SHAP importance of concrete and soil thermal conductivities over time, with the mean t*, t*/4 and 9t*/4 overlaid

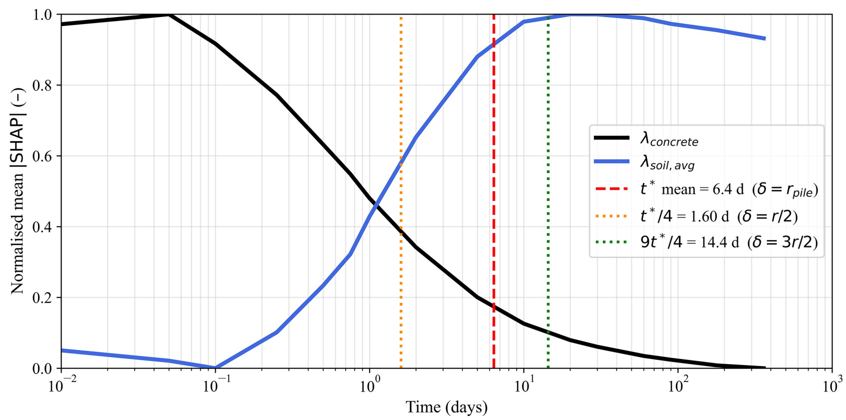

evolving from the pile to the surrounding ground. Between the two boundaries, the mean absolute SHAP importance of $\lambda_{\mathrm{concrete}}$ decreases by 44%, while that of $\lambda_{\mathrm{soil,avg}}$ increases by 36%. The crossover between the normalised mean SHAP values for $\lambda_{\mathrm{concrete}}$ and $\lambda_{\mathrm{soil,avg}}$ occurs near t*/4 (i.e. $\delta = \mathrm{r_{pile}}/2$), reflecting the impact of placing the heat exchanger pipes close to the edge of the pile: the effective conduction distance from the pipe wall to the pile–soil interface is smaller than $\mathrm{r_{pile}}$, and the crossover near t*/4 is therefore consistent with the thermal front reaching the pile-soil interface earlier than the characteristic time t*, which was calculated using the pile radius, would suggest.

Figure 13 presents the mean absolute SHAP values for the thermal response surrogate, normalised by the sum of mean values across all features. This shows the importance of each input feature in predicting the normalised wall (Φ_{wall}) and outlet (Φ_{outlet}) responses in the short ($t = 1$ *day*) and long ($t = 1000$ *days*) terms. The features are ranked based on the outlet Day 1 importance to highlight the evolution of their influence over time.

The most relevant observation is the minimal contribution of the initial temperature ($T_{initial}$) and the applied heat flux ($\overline{q_{flux}}$), confirming that the normalised thermal responses are purely geometry- and material-dependent.

Similarly, the fluid velocity (v_{fluid}) shows negligible relevance for the wall response and only a small effect on the outlet, reflecting that the system operates under a prescribed heat-flux boundary condition rather than a fixed inlet temperature.

For the wall response, the pile diameter (D_{pile}) is by far the most influential feature at all times. A larger diameter increases the perimeter through which heat is exchanged, effectively reducing the average temperature change for a given heat input. This observation highlights a key limitation of analytical g-function formulations, namely that changes in pile geometry require a re-evaluation of the thermal response, making generalised analytical expressions difficult to establish without case-specific analysis. In this context, the proposed surrogate offers a practical advantage by enabling rapid re-computation of the wall thermal response across a wide range of pile geometries without the need for repeated detailed modelling. The soil thermal conductivity ($\lambda_{soil,avg}$) also gains importance as time increases, since the long-term temperature field is dominated by radial heat diffusion in the surrounding soil. The apparent influence of the pile length (L_{pile}) at later times, reflects the contribution of end effects captured in the three-dimensional FE model. These effects slightly enhance the surrogate model's sensitivity to the pile's total length in the long term.

In contrast, for the outlet response, the number of loops (n_{loops}) emerges as the dominant factor across all time scales, as it directly governs the length of pipe and therefore promotes greater heat transfer from the pipe to the surrounding concrete, resulting in lower outlet temperatures. This parameter directly governs the total heat exchange surface and the internal hydraulic configuration, thereby exerting a major influence on the mean outlet temperature. The concrete and soil thermal

Figure 13 Normalised mean SHAP values for the wall and outlet thermal response surrogate for Days 1 and 1000

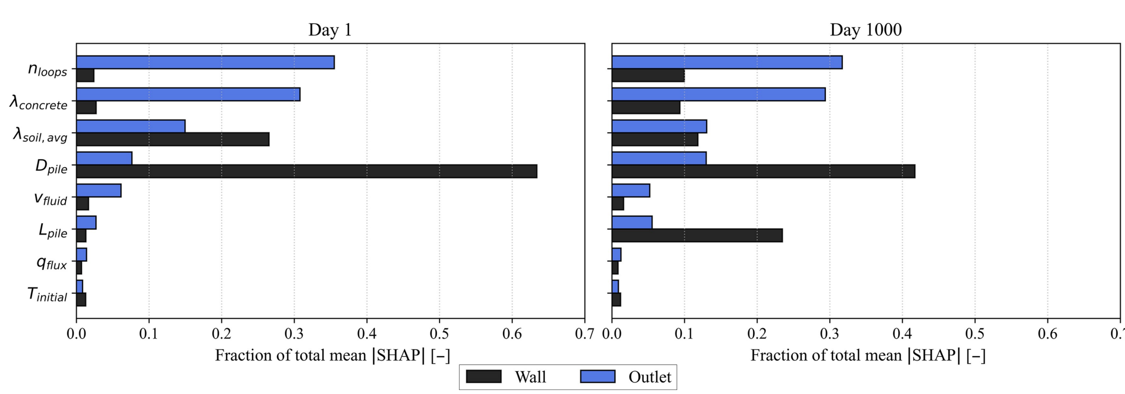

conductivities ($\lambda_{concrete}$) and ($\lambda_{soil,avg}$) also retain high importance throughout, as they control the combined conductive resistance between the heat source and the ground. The pile diameter maintains a secondary but consistent influence on the outlet predictions in both the short and long terms.

6. Case studies

To evaluate the outlet surrogate model against field measurements, the thermal response test (TRT) reported by Loveridge *et al.* (2014) was used as a benchmark for combined heating, cooling and recovery cycles. The tested pile has a diameter of 300 mm (smaller than the minimum 500 mm diameter represented in the surrogate training set) and a total length of 26.8 m, of which 26 m corresponds to the single U-loop. The concrete thermal conductivity was taken as 2.0 W m^{-1} K^{-1}, as suggested in Gawecka *et al.* (2020), while an average soil conductivity of 2.6 W m^{-1} K^{-1} was adopted, consistent with the value identified in Loveridge *et al.* (2014). Figure 14 presents the comparison between the field data and the thermal response surrogate predictions obtained through superposition of individual g-function pulses corresponding to the four TRT stages (heating, recovery, cooling and recovery).

The surrogate accurately reproduces the field thermal response throughout the first three stages, with only a slight underestimation during the final recovery period, further supporting the validity of the surrogate predictions and generalisation capabilities despite the pile geometry falling outside the surrogate's training range. Nevertheless, extrapolation beyond the trained parameter space should be treated with caution, and engineering judgement, independent validation and high-fidelity simulation are recommended before applying the surrogate in such cases.

A constant temperature TRT was not performed on this pile, so a direct comparison with the power output surrogate is therefore not possible. However, for a constant inlet temperature 15 °C below the initial ground temperature, the surrogate predicts an initial power output of approximately 45.6 W/m after 10 days, gradually reducing to a steady-state value of 33.4 W/m. These values are consistent with design guidance and published numerical results for comparable pile geometries. Brandl (2006) recommends 40–60 W/m for piles with diameters in the 0.3–0.5 m range, while Laloui and di Donna (2011) report a broader operational range of 20–100 W/m, depending on ground conditions and pile configuration. The surrogate predictions therefore fall comfortably within both intervals.

To provide a direct validation of this power output surrogate under a constant inlet temperature boundary condition, the Thermal Performance Test reported by You *et al.* (2021) was used as a benchmark. The tested pile had a diameter of 0.8 m, a length of 20 m and two pipe loops, with a constant inlet temperature of 5 °C. The surrogate was evaluated using an average soil thermal conductivity of 1.2 W m^{-1} K^{-1} and a concrete thermal conductivity of 1.25 W m^{-1} K^{-1}, with the remaining inputs set to match the reported experimental configuration. Figure 15 presents the comparison between the field measurements and the surrogate predictions for the first 30 h of operation.

The surrogate reproduces the measured behaviour, which, as expected in transient heat extraction problems, can be separated into two distinct stages: an initial steep decline as heat diffuses radially through the pile concrete, followed by a more gradual reduction of the power output as the thermal front propagates into the surrounding soil, reducing the temperature gradient driving heat diffusion. Agreement with the experimental data is good from early stages of the test (>1 h), with the predicted decay closely tracking the measurements through the test. The slight underestimation during the first hour is consistent with the known early-time limitations of the surrogate discussed earlier, and is of limited consequence for design, where performance assessments are governed by behaviour over longer periods.

7. Conclusions

Thermo-active piles can help improve the overall sustainability of urban infrastructure. This research presented a method to generalise both the power output and the thermal response functions of thermo-active piles using data-driven surrogate models. These were trained on numerical data generated from two sets of 3D FE simulations with explicitly simulated fluid-flow heat transfer. The following conclusions can be drawn:

- The first surrogate provides power output per unit length predictions for the first year of operation and in the very long term (i.e. steady state), considering a constant inlet

Figure 14 Comparison of wall and outlet temperatures obtained from a field TRT and the surrogate model

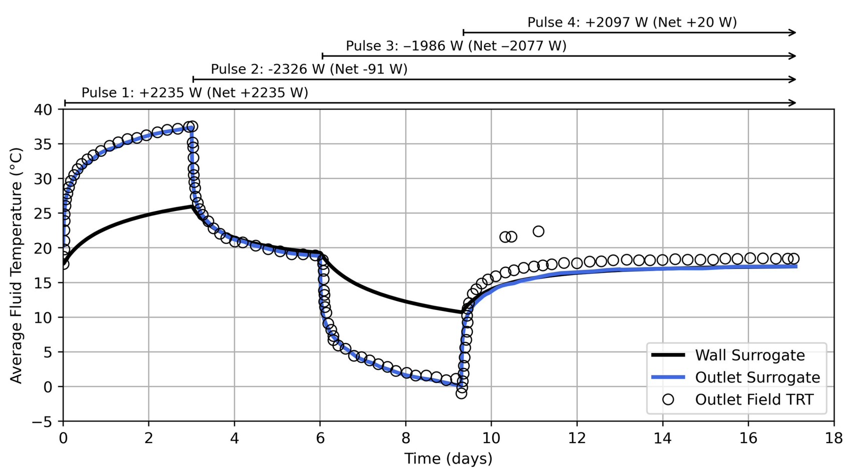

Figure 15 Comparison of power output results from a field TPT and the surrogate output

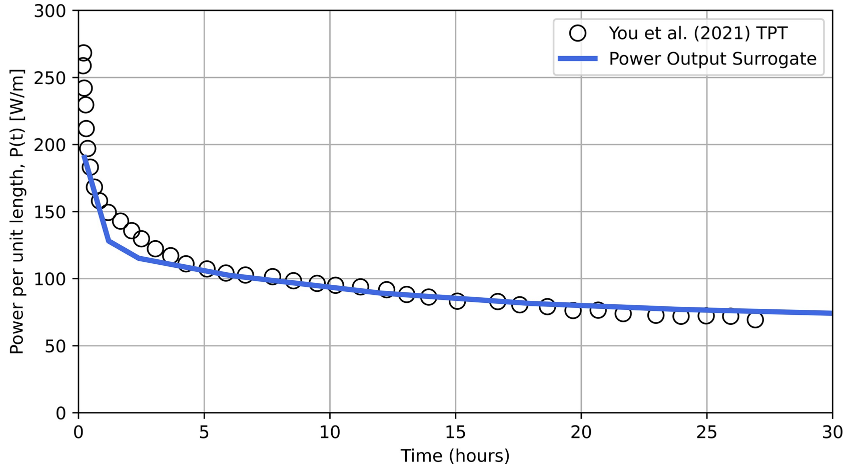

temperature. The model achieves a very high predictive accuracy across the entire time domain, with R^2 values exceeding 0.99 and MAEs below 2 W/m for $t > 1$ *day*. The surrogate captures both the early steep variation in power output and the later flattening of the power curve with an average MRE of 4.4%, demonstrating excellent agreement with the underlying FE data.

- The second surrogate predicts the normalised thermal responses for the pile wall and outlet over a 10-year period for an applied constant heat flux. Both models show very strong agreement with the reference numerical simulations, with global per-point R^2 values of 0.994–0.997. When assessed on an average per-timestep basis, the wall and outlet responses retain high accuracies of 0.971 and 0.959, respectively. The model reproduces the characteristic logarithmic growth of the g-function over several orders of magnitude, with errors largely remaining within engineering-acceptable limits.
- The surrogate predictions exhibit consistent behaviour over the full time range. The initial steep rise in thermal response is accurately captured, while small deviations appear only for larger time instants. These discrepancies correspond to the transition from a predominantly two-dimensional heat transfer regime to a three-dimensional one, which the numerical FE model resolves but the surrogate can only approximate. Nonetheless, the absolute and relative errors remain small and do not compromise the usefulness of the surrogates.
- The SHAP analysis provides interpretability of the predictions produced by both surrogate models. For power output, the temperature difference and thermal conductivities dominate the prediction in a manner consistent with transient heat-transfer physics. For the thermal response surrogate, the importance of geometric and material parameters aligns with the behaviour expected of g-functions, further supporting the robustness and physical consistency of the models.
- Validation against a multi-stage TRT from Loveridge et al. (2014) demonstrated excellent agreement between the surrogate predictions and field-measured temperatures, highlighting strong model generalisation beyond the trained diameter range.

Together, the two surrogates provide a coherent framework capable of defining the thermal behaviour of a wide range of single thermo-active piles, with varying geometries, material properties and hydraulic configurations. Within these bounds, the surrogates enable rapid exploration and conceptual design of pile heat-exchanger systems without the need for high-fidelity FE simulations, contributing to the wider adoption of thermo-active foundations and supporting the transition of the built environment towards net-zero targets. Moreover, it should be noted that, although the present framework is limited to isolated single piles, an extension to groups of thermo-active piles – outside the scope of this work – is possible by combining directly the produced surrogate models with the thermal interaction factors-based procedure proposed in Liu and Taborda (2024a) and Liu and Taborda (2024b).

Author contributions

Javier Sánchez Fernández – Data curation (Lead), Formal analysis (Equal), Investigation (Lead), Methodology (Lead), Writing – original draft (Lead), Writing – review and editing (Supporting). Agustin Ruiz López – Conceptualisation (Supporting), Methodology (Supporting), Supervision (Equal), Writing – review and editing (Equal). David M.G. Taborda – Conceptualisation (Lead), Methodology (Supporting), Project Administration (Lead), Supervision (Equal), Writing – review and editing (Equal).

Data availability

The power output and g-function prediction surrogates and data sets are available in Sánchez Fernández (2026).

References

Bourne-Webb, P.J., Amatya, B. and Soga, K. (2013), "A framework for understanding energy pile behaviour", *Proceedings of the Institution of Civil Engineers - Geotechnical Engineering*, Vol. 166 No. 2, pp. 170-177, doi: 10.1680/geng.10.00098.

Bourne-Webb, P., Burlon, S., Javed, S., Kürten, S. and Loveridge, F. (2016), "Analysis and design methods for energy

geostructures", *Renewable and Sustainable Energy Reviews*, Vol. 65, pp. 402-419, doi: 10.1016/j.rser.2016.06.046.
Brandl, H. (2006), "Energy foundations and other thermo-active ground structures", *Géotechnique*, Vol. 56 No. 2, pp. 81-122, doi: 10.1680/geot.2006.56.2.81.
Cecinato, F. and Loveridge, F. (2015), "Influences on the thermal efficiency of energy piles", *Energy*, Vol. 82, pp. 1021-1033, doi: 10.1016/j.energy.2015.02.001.
Chollet, F. (2021), *Deep Learning with Python*, United States, Manning Publications, New York, NY.
COMSOL Multiphysics (2021), "Heat transfer in pipes - the heat transfer equation", available at: https://doc.comsol.com/6.0/doc/com.comsol.help.pipe/pipe_ug_heattransfer.06.16.html#568028 (accessed 17 December 2025).
D'Agostino, D., Mele, L., Minichiello, F. and Renno, C. (2020), "The use of ground source heat pump to achieve a net zero energy building", *Energies*, Vol. 13 No. 13, pp. 1-21, doi: 10.3390/en13133450.
Eskilson, P. (1987), "Thermal analysis of heat extraction boreholes", Doctoral Thesis (compilation). Department of Physics.
Gawecka, K.A., Taborda, D.M.G., Potts, D.M., Cui, W., Zdravkovic, L. and Haji Kasri, M.S. (2017), "Numerical modelling of thermo-active piles in London clay", *Proceedings of the Institution of Civil Engineers - Geotechnical Engineering*, Vol. 170 No. 3, pp. 201-219, doi: 10.1680/jgeen.16.00096.
Gawecka, K.A., Taborda, D.M.G., Potts, D.M., Sailer, E., Cui, W. and Zdravković, L. (2020), "Finite-element modeling of heat transfer in ground source energy systems with heat exchanger pipes", *International Journal of Geomechanics*, Vol. 20 No. 5, pp. 1-14, doi: 10.1061/(asce)gm.1943-5622.0001658.
Geron, A. (2019), *Hands-on Machine Learning with Scikit-Learn, Keras and TensorFlow: concepts, Tools, and Techniques to Build Intelligent Systems*, 2nd ed., O'Reilly, Sebastopol, CA.
Imtiyaz, P.A., Khalad, A. and Muqtadir, S.A. (2023), "Prediction of thermal conduction of energy piles using various machine learning models", *International Journal of Geotechnical Engineering*, Vol. 17 No. 6, pp. 668-680, doi: 10.1080/19386362.2024.2362024.
Laloui, L. and di Donna, A. (2011), "Understanding the behaviour of energy geo-structures", *Proceedings of the Institution of Civil Engineers - Civil Engineering*, Vol. 164 No. 4, pp. 184-191, doi: 10.1680/cien.2011.164.4.184.
Laloui, L., Nuth, M. and Vulliet, L. (2006), "Experimental and numerical investigations of the behaviour of a heat exchanger pile", *International Journal for Numerical and Analytical Methods in Geomechanics*, Vol. 30 No. 8, pp. 763-781, doi: 10.1002/nag.499.
Liu, R.Y.W. and Taborda, D.M.G. (2023), "A simplified methodology for determining the thermal performance of thermo-active piles", *Environmental Geotechnics*, doi: 10.1680/jenge.22.00119.
Liu, R.Y.W. and Taborda, D.M.G. (2024a), "A methodology for incorporating thermal interference in the design of thermo-active pile groups", *Geomechanics for Energy and the Environment*, Vol. 39, p. 100575, doi: 10.1016/j.gete.2024.100575.
Liu, R.Y.W. and Taborda, D.M.G. (2024b), "The effects of thermal interference on the thermal performance of thermo-active pile groups", *Renewable Energy*, Vol. 225, p. 120357, doi: 10.1016/j.renene.2024.120357.
Loveridge, F. and Powrie, W. (2013), "Temperature response functions (G-functions) for single pile heat exchangers", *Energy*, Vol. 57, pp. 554-564, doi: 10.1016/j.energy.2013.04.060.
Loveridge, F. and Powrie, W. (2014), "G-Functions for multiple interacting pile heat exchangers", *Energy*, Vol. 64, pp. 747-757, doi: 10.1016/j.energy.2013.11.014.
Loveridge, F., Powrie, W. and Nicholson, D. (2014), "Comparison of two different models for pile thermal response test interpretation", *Acta Geotechnica*, Vol. 9 No. 3, pp. 367-384, doi: 10.1007/s11440-014-0306-3.
Lundberg, S.M. and Lee, S.I. (2017), "A unified approach to interpreting model predictions", *Advances in Neural Information Processing Systems*, pp. 4766-4775.
McKay, M.D., Beckman, R.J. and Conover, W.J. (1979), "A comparison of three methods for selecting values of input variables in the analysis of output from a computer code", *Technometrics*, Vol. 42 No. 1, pp. 55-61, doi: 10.1080/00401706.2000.10485979.
Makasis, N., Narsilio, G.A. and Bidarmaghz, A. (2018), "A machine learning approach to energy pile design", *Computers and Geotechnics*, Vol. 97, pp. 189-203, doi: 10.1016/j.compgeo.2018.01.011.
Makasis, N., Narsilio, G.A., Bidarmaghz, A., Johnston, I.W. and Zhong, Y. (2020), "The importance of boundary conditions on the modelling of energy retaining walls", *Computers and Geotechnics*, Vol. 120, p. 103399, doi: 10.1016/j.compgeo.2019.103399.
Wang, C., Dong, S., Bouazza, A. and Ding, X. (2025), "Explainable machine learning models to predict outlet water temperature of pipe-type energy pile", *Renewable Energy*, Vol. 246, p. 122972, doi: 10.1016/j.renene.2025.122972.
You, S., Wang, Y.T. and Jiang, P. (2021), "Operation mode and heat performance of energy drilled piles", *Thermal Science*, Vol. 25 No. 6, pp. 4553-4560, doi: 10.2298/TSCI2106553Y.
Zhang, Q., Zhou, X., Sun, D., Gao, Y., Wen, M., Hu, S. and Gong, N. (2025), "Analytical heat transfer model of energy piles in layered and anisotropic soils considering interfacial thermal resistance", *International Journal of Thermal Sciences*, Vol. 217, p. 110115, doi: 10.1016/j.ijthermalsci.2025.110115.
Zhang, W., Zhou, H., Bao, X. and Cui, H. (2023), "Outlet water temperature prediction of energy pile based on spatial-temporal feature extraction through CNN–LSTM hybrid model", *Energy*, Vol. 264, p. 126190, doi: 10.1016/j.energy.2022.126190.

Corresponding author

Javier Sánchez Fernández can be contacted at: js8918@ic.ac.uk